











# Modified qHAADF method for atomic column-by-column compositional quantification of semiconductor heterostructures

Atif A. Khan<sup>1,\*</sup> , M. Herrera<sup>1</sup> , J. Pizarro<sup>2</sup> , P. L. Galindo<sup>2</sup> , P. J. Carrington<sup>3</sup> , H. Fujita<sup>4,5</sup> , A. Krier<sup>4</sup> , and S. I. Molina<sup>1</sup> 

<sup>1</sup>Department of Material Science, Metallurgical Chemistry and Inorganic Chemistry, IMEYMAT, University of Cádiz, 11510 Puerto Real, Spain

<sup>2</sup>Department of Computer Engineering, ESI, University of Cádiz, 11510 Puerto Real, Spain

<sup>3</sup>Department of Engineering, Lancaster University, Lancaster LA1 4YW, UK

<sup>4</sup>Physics Department, Lancaster University, Lancaster LA1 4YB, UK

<sup>5</sup>Asahi Kasei Corporation, 2-1 Samejima, Fuji-City, Shizuoka 416-8501, Japan

Received: 28 May 2018

Accepted: 23 October 2018

Published online:

15 November 2018

© Springer Science+Business Media, LLC, part of Springer Nature 2018

## ABSTRACT

The qHAADF method allows the quantification of the composition at atomic column resolution in semiconductor materials by comparing the HAADF-STEM intensities between a region of interest to a region of the material of known composition. However, the application of this qHAADF approach requires both regions to be differentiable and included in the same micrograph at close proximity. This limits the application of this approach to certain materials and magnifications where this requirement is fulfilled. In this work, we extend the qHAADF method to analyses where the reference region is imaged in a separate micrograph. The validity of this modified method is proved by comparison to the original qHAADF approach using HAADF-STEM simulated images of the semiconductor heterostructure InSb/InAs. Additionally, the methods are applied successfully to experimental images both of a simple InSb/InAs interface and of a complex InSb/GaSb heterostructure, justifying the significance of the modified method over the original method.

## Introduction

High angle annular dark field (HAADF)–scanning transmission electron microscopy (STEM) [1] is widely used for the investigation of the morphology and composition of materials at atomic scale [2–5].

The analysis of single dopant atom in crystalline structures [6], defects within structures [7], interfacial discontinuity [8–10] or structural strain [11] are some of the advantageous outcomes of this method. In some materials, the study of the composition at atomic scale is essential to understand their

Address correspondence to E-mail: atif.khan@uca.es

performance. This is the case of semiconductor materials where, for example, the emission wavelength of InGaAsN laser can be tuned within 1.2–1.6  $\mu\text{m}$  by manipulating In and N incorporations [12]. In InSbAs, the control of the distribution Sb–As allows the design of type II quantum dots (QDs) [13] based highly efficient mid-infrared optoelectronic devices at a wavelength range of 2–8  $\mu\text{m}$  [14]. Because of this, HAADF-STEM has been widely used for the analysis of III–V [15] and II–VI [16] semiconductor heterostructures. As an example, the effect of the capping layer in the morphology of InAs/GaAs QDs [17] has been demonstrated using this technique. In semiconductor materials, quantifying the composition with large spatial resolution is needed to correlate material band structure and epitaxial growth conditions, which eventually assists the extrapolation of optimum device design parameters. Several direct and indirect analyzing techniques have been used in this regard such as photoluminescence (PL) [18, 19], energy dispersive spectroscopy (EDS) [20] or electron energy loss spectroscopy (EELS) [21, 22]. HAADF-STEM can also be used with this purpose, although the quantification is not straightforward as the HAADF-STEM signal contains both composition and specimen thickness induced information [23, 24]. Several methodologies have been developed in order to obtain quantitative information using (HA)ADF-STEM images. For example, a setup has been built to exploit the explicit angular dependence of scattered intensity for angle-resolved STEM to measure N content and specimen thickness in  $\text{GaN}_x\text{As}_{1-x}$  [25]. Also, a method is proposed to normalize HAADF-STEM intensity to the incident electron beams in order to quantify ADF images [24, 26, 27]. Additionally, it has been shown that empirical incoherent parametric imaging can be combined with frozen lattice multislice simulations in order to evolve from a relative toward an absolute quantification of the composition of single atomic columns [28]. Although these methodologies have been shown to provide reliable results, they either require time consuming multiple experimental analyses in terms of variable image acquisition parameters or require additional complex instrumentation or not compatible to material segregation associated compositional quantification. As a result, a direct and faster compositional quantification model of quantitative HAADF (qHAADF) [29] has been developed that compares experimental HAADF-STEM

integrated intensities of the region of interest (ROI) with the intensity of a homogenous (reference) area to quantify the composition [30], using a single set of image acquisition parameters. For example, the compositional distribution of Sb has been quantified within GaAs capped GaSb nanostructures [22] and in GaAsSbN capped InAs quantum dots (QDs) [31] using this method. However, this program only works when the ROI and reference regions are at the same HAADF-STEM image. This basic requirement limits this method to function in low magnification in terms of multilayered structures, where the ROI and the reference area (typically, substrate) could be positioned far away from each other. Moreover, in the compositional quantification of highly segregating materials like Sb [32], locating a homogenous region is rather complicated, restraining functionality to this method.

In this paper, a modified version of the qHAADF program is presented. This version compares the integrated intensities of a ROI area to a homogenous (reference) area present in two separate HAADF-STEM images in order to generate a compositional map on the ROI image. The InSb/InAs material is considered to exemplify the method. Primarily, the compositional outcomes of the modified method applied to simulated InSb/InAs images are compared to the existing qHAADF method using various image-pixel accumulation areas (integration areas), and to the real composition in the simulated models, proving its validity. Later, the compatibility of the modified method to the original method is demonstrated in terms of experimental HAADF-STEM InAs/InSb<sub>x</sub>As<sub>1-x</sub>/InAs images. As the final demonstration, another experimental HAADF-STEM image of alternating InSb/GaSb structure is considered which can potentially be analyzed by the modified method due to the absence of a reference region close to the ROI.

## Materials and methods

The first experimental sample consists of an InSb/InAs heterostructure, grown on an InAs [001] substrate using molecular beam epitaxy (MBE) technique. This sample possesses 10 InSb layers of 1.4 ML each, where two consecutive InSb layers are separated by an InAs layer of 18 nm in between. The second experimental sample accommodates a 30 ML

thick MBE (001) grown QD layer, comprised of alternating sub-monolayer (SML) InSb/GaSb structure. This sample has been selected as an example because the existing qHAADF method assisting compositional quantification of In within this QD layer with the help of a homogeneous buffer layer of GaSb is rather impossible due to a presence of a very thick (1.5  $\mu\text{m}$ )  $\text{Al}_{0.3}\text{Ga}_{0.7}\text{Sb}$  barrier layer in between and hence justifies the importance of developing the modified method.

The electron transparent specimens for the HAADF-STEM analysis associated with both samples were prepared by mechanical thinning and Precision Ion Polishing System (PIPS) associated  $\text{Ar}^+$  ion milling. All experimental high-resolution HAADF-STEM images of the prepared specimens were obtained using a JEOL JEM ARM 200cF single aberration corrected (condenser aberration) microscope working at an operating voltage of 200 kV, while having imaging parameters of  $C_s = -611$  nm,  $C_5 = 817.2$  mm, HAADF detector inner angle = 90 mrad, objective aperture angle = 15.2 mrad and defocus =  $-1$  Å.

Simulated HAADF images of InAs/InSb/InAs structures along [110] zone axis have been computed using the model illustrated in Fig. 1 where As columns are included as blue circles, In as cyan circles and Sb as yellow circles. In each simulated model, Sb columns are included within 3 central monolayers (MLs) as shown in Fig. 1, with partial presence of As ( $\text{InSb}_x\text{As}_{1-x}$ ). Here, the nominal Sb composition ( $x$ ) is varied from 0 to 0.5 with 0.1 increment. All the simulations were performed using SICSTEM software that runs on CAI supercomputer in UCA. The working principle of the SICSTEM software can be found here [33]. Aberration correction associated spatial incoherence was also considered during simulations [34].

## Results and discussion

### Implementation of the method

In order to exemplify the application of the modified qHAADF method, two simulated images of InAs/InSb<sub>*x*</sub>As<sub>1-*x*</sub>/InAs ([001]) have been chosen where the nominal Sb composition at the ROI image is 50% ( $x = 0.5$ ) and at the reference image is 0% ( $x = 0$ ), with specimen thickness of 20 nm. As the first processing step, individual local intensity maxima

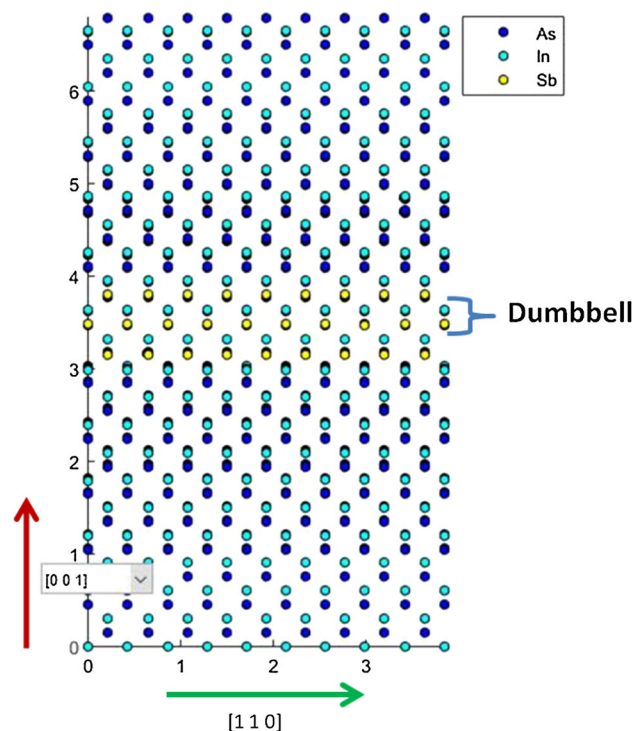
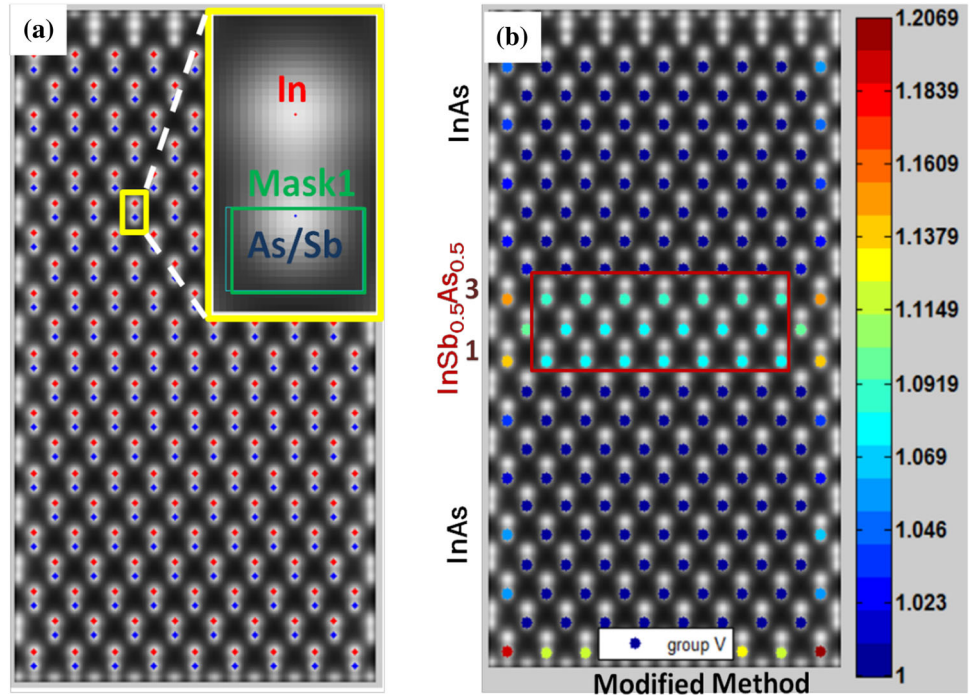


**Figure 1** Schematic of the model used for the simulation of the InAs/InSb/InAs layers.

associated with the group III and V atomic columns are located within each HAADF-STEM image. This is done using a peak finding (PF) technique, used by Pedro L. Galindo et al. while developing the Peak Pairs (PP) method [35]. Figure 2a shows a simulated HAADF-STEM image of the ROI (the Sb containing layer) with PF generated peaks, where the group III (In) atomic columns are marked with red dots and the group V (As/Sb) columns with blue dots. For clarity, the inset shows a single III–V pair (dumbbell) with separate group III (red) and group V (blue) column peaks. In our case, the atomic columns with variable composition are the group V ones so they are the columns of interest. In order to measure the intensity in these columns, integration areas are chosen around the group V intensity maxima. In this case, an integration area containing the same part of the atomic column as proposed in [36] has been chosen with different pixel numbers justifying the corresponding image resolution (see the green rectangle included in the inset of Fig. 2a), which is reported to possess least susceptibility to the effects of the neighboring group III columns. This integration area can be named as Mask 1. As the first calculation step, the pixel intensities are integrated

**Figure 2** **a** HAADF-STEM simulated image of  $\text{InSb}_{0.5}\text{As}_{0.5}$  where the group III (In) atomic columns are marked with red dots and the group V (As/Sb) atomic columns with blue dots. The inset represents a single dumbbell where a group V atomic column is surrounded by a Mask1 (green rectangle). **b** The modified qHAADF method generated ‘R’ map corresponds the image in **a**. The red rectangle represents the  $\text{InSb}_{0.5}\text{As}_{0.5}$  area.



within Mask 1 areas on each dumbbell individually on the ROI image. With regards to the reference image, it has been taken as the HAADF-STEM image that contains only InAs dumbbells (known composition). Similarly to the procedure explained above for the ROI image, the Mask 1 containing pixel intensities around each group V (As) atomic columns integrated on the reference image and later these integrated intensities from all group V (As) columns are averaged. Finally, the integrated intensities from each group V column on the ROI image are divided by the average of the integrated intensities from the group V columns on the reference image. These outcomes on the ROI image can be termed as normalized integrated intensities,  $R$ . Figure 2b represents the modified qHAADF program originated ‘R’ map corresponding to the group V columns (As/Sb) included in Fig. 2a. In this map,  $R = 1$  (deep blue dots) depicts the absence of Sb (InAs atomic columns). The red rectangle marks the dumbbells within the three  $\text{InSb}_{0.5}\text{As}_{0.5}$  MLs, where an average ‘R’ value of  $\sim 1.08$  has been measured. It should be noted that the unrealistic and relatively higher ‘R’ values associated with the dumbbells nearer to the image boundaries must not be taken into account as those contain simulation originated boundary errors.

In order to assess the validity of the modified method, it has been compared to the original

qHAADF method. For this, InAs dumbbells from the same image of  $\text{InSb}_{0.5}\text{As}_{0.5}$  analyzed have been taken as the reference region for the calculation, and the same Mask 1 has been used while having the sample thickness of 20 nm. Our results have shown that the original method generates same ‘R’ values over same group V columns (not shown) as in Fig. 2b. This outcome confirms that for a homogenous and same ROI-reference thickness, the modified method is compatible with the original method in terms of simulated images.

To analyze the efficiency of the modified method, the deviation of Sb composition values obtained from the qHAADF methods with regards to the nominal composition need to be evaluated. This requires converting the Sb contribution associated ‘R’ values within the InSbAs layers into composition values. For this, we have used the atomic column-by-column quantification approach developed in [29]. Here, a statistically obtained linear regression equation was proposed to quantify column-by-column As composition from ‘R’ or ‘ $R_i$ ’ values, associated with experimental  $\text{InAs}_x\text{P}_{1-x}/\text{InP}$  structure. The proposed equation is

$$R_i = 1 + a \cdot x_i \tag{1}$$

where  $x_i$  represents As composition. They obtained the constant ‘a’ value by evaluating an As-based



statistical  $R_i$  versus  $x_i$  graph in terms of a few known  $x_i$  compositions. They have also experimentally ensured that the effect of certain range of sample thicknesses over ' $R_i$ ' values is insignificant and hence, the variation in  $x_i$  is the only effective contributing parameter here. Later on, the validity of the above mentioned equation was justified at [36] for other III–V ternary alloys. Here, the researchers proposed a direct approach to obtain the constant ' $a$ ' value by summing monolayer-by-monolayer average ' $R_i$ ' values within certain number of MLs ( $N$ ), where the both analyzing and reference materials must be present at the same HAADF-STEM image. Their proposed equation was

$$\sum_{i=1}^N R_i = N + a \cdot \sum_{i=1}^N x_i. \quad (2)$$

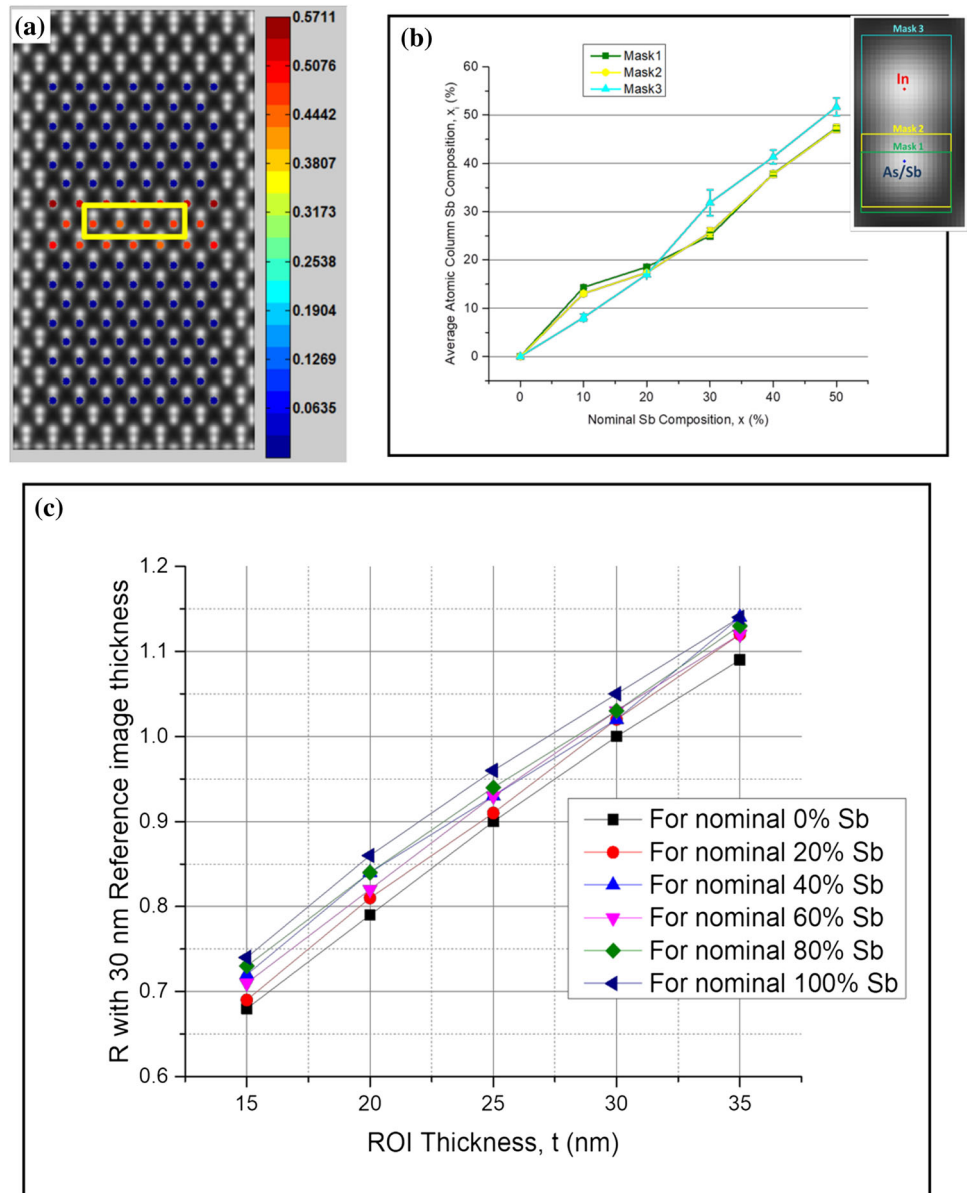
This equation illustrates the total change in the  $R_i$  value due to total deposition of  $x_i$  within certain number of MLs ( $N$ ). This equation provides the ' $a$ ' value, which later can be used to obtain average monolayer-by-monolayer or column-by-column  $x_i$  values.

We have applied the methodology above for the quantification of Sb in our simulated HAADF images using the ' $R$ ' values obtained with the modified method shown in Fig. 2b. Initially, ' $a$ ' has been obtained using total deposited  $x_i$  values and corresponding average monolayer-by-monolayer  $R_i$  values within  $N$  MLs. For that, 17 MLs in the ROI image have been chosen ( $N = 17$ ) as it ensures that the 3 Sb containing MLs are present within that 17 MLs while ignoring the simulation oriented boundary errors. Next, the obtained ' $a$ ' value is used in the first equation and Sb associated column-by-column local composition map is generated. Figure 3a represents the column-by-column local composition values calculated for the image corresponding to  $\text{InSb}_{0.5}\text{As}_{0.5}$  through red dots. Here, to maintain simplicity evaluating the Mask1 associated deviation between the nominal ( $x = 0.5$ ) and calculated values, four central group V columns have been chosen, represented within a yellow rectangle. The obtained average value of Sb composition associated with those four dumbbells has been found to be 47.38% with a standard estimation error of 3.77%. This error falls within 99.9% of confidence level to the average value associated with statistical two-sided  $t$ -distribution, signifying that the composition of  $47.38 \pm 3.77\%$  assures

99.9% certainty to the true (nominal) value. In order to determine whether this method is also good for other nominal compositions, column-by-column Sb composition quantification maps have been generated for the Sb nominal values of  $0.1 \leq x \leq 0.4$  (not shown) with 0.1 increment. Figure 3b shows a graph of the average atomic column Sb composition ( $x_i$ ) versus nominal Sb composition associated with Mask1 for images with  $0 \leq x \leq 0.5$  (in green). Here, the Mask1 based overall standard error obtained from the calculated profile (Mask1) is found to be only 4.37%, assuring that the modified qHAADF method is in a good agreement with the expected values in terms of all nominal compositions of  $0 \leq x \leq 0.5$ .

It should be noted that, as suggested by Jones [37], Mask size can be influential in terms of compositional quantification. However, there is no agreement in the literature regarding which mask would be more appropriate for composition quantification. For example, Mask1 functions appropriately in terms of very thin samples, ranging from 15 to 40 nm [34] since the investigating atomic column stays unaffected by the surrounding dumbbells in this thickness range [29]. On the other hand, some researchers suggested a Mask that contains the whole analyzing atomic column proving to provide better HAADF quantitative approach in terms of varying convergence angle, magnification, source size and defocus [38], sample associated small mis-tilt [39], aberrations and astigmatism [40] and scan induced noises [41], as long as the probe size does not change with the sample thickness. These characteristics allow possibility analyzing even thicker samples than of Mask1. In addition, another Mask has been suggested that imposes rectangular Voronoi cell [42] around each whole dumbbell that allows analyzing even thicker samples by providing an average value closer to the nominal [37]. Moreover, for a HAADF-STEM detection angle of 90 mrad, these Voronoi cells are sensitive to sample thickness induced effect [25] and hence, compositional quantification with a higher precision is expected as the thickness contribution to the HAADF-STEM signal can be identified. Because of these arguments, along with Mask1, the modified qHAADF program has been examined with two other Mask sizes, termed as Mask2 (covers each whole group V column) and Mask3 (covers each whole dumbbell) in terms of simulated images, while both ROI and reference images possess same

**Figure 3** **a** Atomic column composition map calculated from the modified qHAADF originated ‘*R*’ values shown in Fig. 2b, superimposed to the HAADF-STEM simulated image. **b** Graph of the average atomic column Sb composition calculated from the modified qHAADF originated ‘*R*’ values versus the nominal Sb composition for the three masks considered. The error bars illustrate standard deviations to the corresponding averages. The inset represents the three mask areas considered: Mask1 (green), Mask2 (yellow) and Mask3 (cyan), surrounding a single In–As/Sb dumbbell.



specimen thickness of 20 nm. Figure 3b shows Mask1 (green), Mask2 (yellow) and Mask3 (cyan) originated graphs in terms of the average atomic column Sb compositions ( $x_i$ ), associated with the same dumbbells within the yellow rectangle as in Fig. 3a versus varying nominal Sb composition ( $0 \leq x \leq 0.5$ ). For clarity, Fig. 3b includes an inset showing a single In–As/Sb dumbbell where the three masks considered have been graphically represented. Here, the Mask1 based overall standard error obtained from the calculated profile (Mask1) is found to be only 4.37%. Again, the overall standard errors corresponding to Mask2 and Mask3 have also been found to be very small as 3.96% and 2.63%, respectively. Thus, our

results show that in terms of simulated HAADF-STEM images with same specimen thickness, the three mask sizes considered are appropriate for the composition quantification. The high level of accuracy obtained could face slight degradation in terms of experimental analysis if the required parameters are not calibrated properly during the image acquisition. For example, to obtain the ‘*R*’ values, it is essential that both the ROI and reference HAADF-STEM images possess same image contrast, brightness and magnification. Once the necessary calibrations are performed, this modified method will offer benefits analyzing high-resolution HAADF-STEM images associated with very high magnifications,

since the ROI and reference regions do not need to be present in the same image. For example, the high-resolution compositional quantification of a highly segregating material such as Sb [32] within a complex micro structure can be performed using this method without finding a pure homogenous area in the same HAADF-STEM image.

It is worth mentioning that the thickness of the sample also plays an essential role in the composition quantification as it has a strong effect on the HAADF-STEM intensity. It has been experimentally proved that the relative normalized integrated intensity 'R', and eventually the composition of a material is hardly affected by the specimen thickness within 15–40 nm [34], as long as both ROI and reference areas exist in the same image and have similar thicknesses [29]. Because of this, in the present paper we address the issue of errors due to the specimen thickness considering the case where the ROI and the reference images correspond to regions of the specimen with different thicknesses. For this, we have measured the R values for InSb<sub>x</sub>As<sub>1-x</sub> (ROI) images with thickness 15–35 nm considering reference InAs regions with average thickness of 30 nm, for Sb compositions of 0% to 100%, and we show the results obtained in Fig. 3c. As observed in this Figure, for each 1 nm increment at the specimen thickness, the R values increase by a factor of  $\sim 0.02 \pm 0.004$  for every Sb composition. For this thickness range, Eq. (1) can be rewritten as

$$R = 1 + a \cdot xi \pm 0.02 \cdot \Delta t \quad (3)$$

As it can be observed, there is a strong effect of  $\Delta t$  on R, indicating that the precise measurement of the thickness of both ROI and reference regions is essential for the precise calculation of the atomic columns composition. However, it is not necessary to use ROI and reference regions with exactly the same thickness, as the calculation of the effect of  $\Delta t$  on R based on simulated images may assist in the quantification of the thickness related intensity modification, allowing a composition value readjustment. This is not inherent to the modified method and should be extended to the original method as well, where sometimes thickness differences can be found in different regions of the same image. However, these thicknesses differences are expected to be more noticeable in the modified method due to the larger distance between ROI and reference regions in the specimen. Therefore, specimen thickness

associated with each experimental HAADF-STEM image must be measured with the highest precision through zero-loss peak EELS analysis.

### Application of the method to InSb/InAs and InSb/GaSb experimental HAADF-STEM images

To understand how this modified method behaves in terms of experimental HAADF-STEM images, it has been applied to a semiconductor heterostructure of InSb/InAs. HAADF-STEM images of this material have been acquired using the same imaging parameters as in the simulated images (included in the section Experimental Details). Initially and in order to select ROI and reference regions with similar thicknesses, the sample has been analyzed at low magnification, as shown in the HAADF-STEM image of Fig. 4a, where the InSb layers can be observed. The corresponding absolute thickness profile along the green line in Fig. 2a at [001] direction is depicted in Fig. 4b, obtained using zero-loss peak EELS analysis. To generate the absolute thickness profile, Gatan digital micrograph software has been used in terms of HAADF-STEM image acquisition specific log-ratio (absolute) parameters associated with electron mean free path (MFP) of  $\sim 59$  nm (calculated using the equations in [43]) at the spectrometer acceptance angle of 90 mrad (semi angle) and alloy specific effective atomic number,  $Z_{\text{eff}}$ . The thickness variation between the average thickness of the ROI region and the average thickness of the reference area in the region of the red rectangle in Fig. 4a has been found to be of  $\sim 1$  nm ( $t_{\text{ROI}} > t_{\text{reference}}$ ), as it can be observed in Fig. 4b. Figure 4c illustrates the atomic column resolution HAADF-STEM image of the ROI region in this area that contains an InSb layer. It should be noted that this image contains the opposite III-V polarity to the simulated images, i.e., the group V (As/Sb) element constitutes the top column of each dumbbell, while the group III (In) element are at the bottom column. The vacuum level signal associated with the microscope detector has been subtracted from the obtained experimental HAADF-STEM images [37] and the noise has been reduced by applying a Wiener filter in Fourier space [44]. In order to detect the position of the InSb layer, Fig. 4d shows an intensity profile obtained from the red rectangle box in Fig. 4c along [001] direction. In each specific ML along [110] direction, each higher peak assigns the



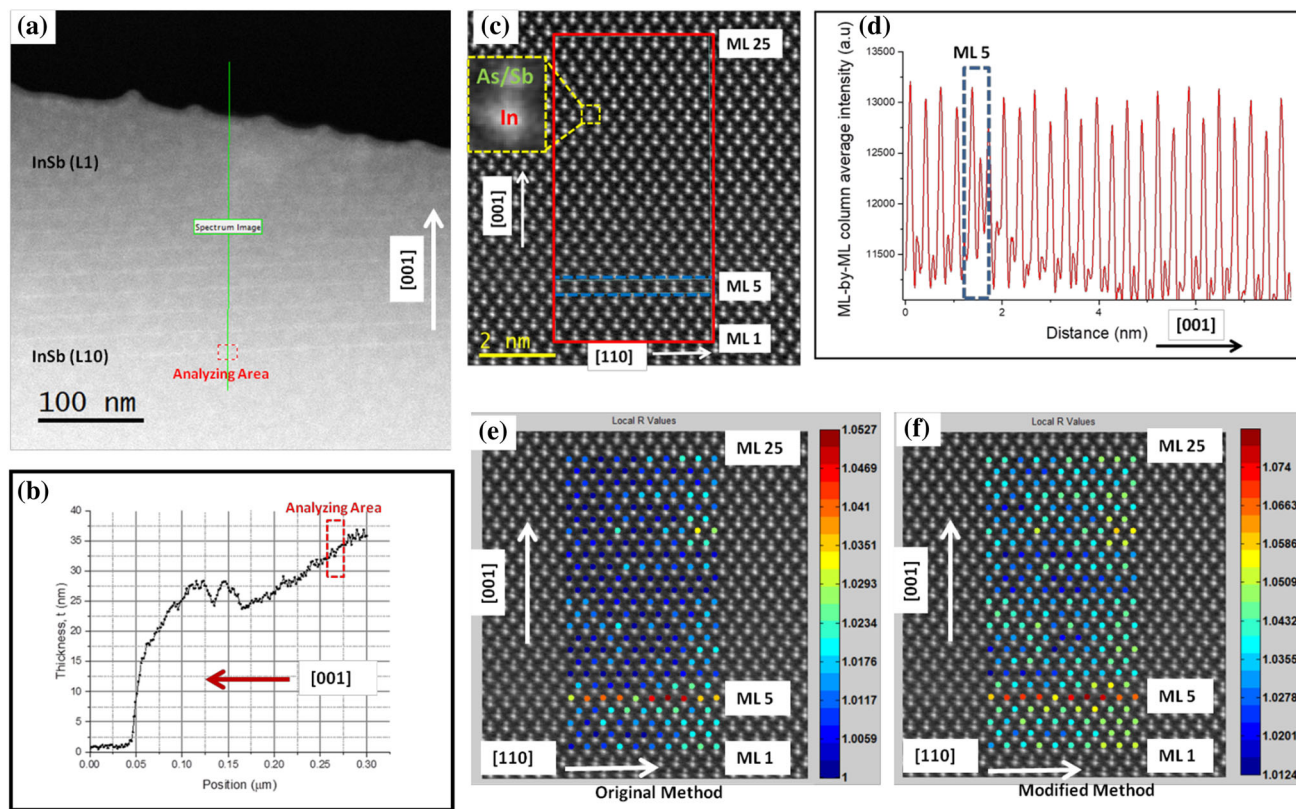


**Figure 4** **a** Low-mag HAADF-STEM image where the red rectangle depicts the location of the analyzing ROI and Reference areas; **b** corresponding thickness profile associated with the Spectrum image line (green line), along with the analyzing area in **a**. **c** Experimental HAADF-STEM image of

InSb/InAs (single In–As/Sb dumbbell at the inset); **d** intensity profile obtained from the image in **c**, evidencing the position of the InSb layer; **R** map calculated with the original **e** and modified **f** methods, from the HAADF-STEM image in **c**.

average intensity from the group III atomic column ( $Z_{In} = 49$ ), and each lower peak designates the average intensity from the group V ( $Z_{As} = 33$ ), within that ML. According to the obtained profile, the average intensity count along [110] direction from the As/Sb columns within ML5 (marked with blue dotted rectangles in Fig. 4a and b) has higher value than any other As/Sb columns, indicating the presence of Sb at ML5. In order to generate a quantitative ‘R’ map from this HAADF-STEM image (ROI image) using the modified qHAADF method, another HAADF-STEM image with same magnification and imaging parameters as in the ROI image has been taken from the InAs substrate in the region of similar thickness (not shown), which will be used as the reference image. Individual local intensity maxima associated with the group III and V atomic columns have been located using previously discussed peak finding (PF) technique, [35] and R values have been calculated similarly as in the simulated images. Figure 4e and f

represents the original and the modified qHAADF method generated ‘R’ maps, respectively. As it can be observed, larger R values are obtained in ML5 in both methods where Sb is present, as expected, with an average value of  $\sim 1.04$  (Fig. 4e) associated with the original method and of  $\sim 1.06$  (Fig. 4f), associated with the modified method where average ROI thickness is greater ( $\sim 1$  nm) than the average reference thickness. Due to this variation in the R values, the corresponding average  $x_i$  at ML5 using equation  $R = 1 + a \cdot x_i$  become  $\sim 27\%$  for the original and  $\sim 46\%$  for modified method. This 16% difference in  $x_i$  between the original and modified method is due to the specimen thickness contribution for  $a \sim 1$  nm ROI-reference average thickness variation in the modified method. As this is a large difference for quantitative purposes, image simulations need to be taken into account to recalculate the obtained values considering the thickness variations measured in order to obtain precise composition values. In order



to do that, in this case Eq. (3) above can be used. For values of  $\Delta t$  of 1 nm and  $R \sim 1.06$ , we obtain a  $x$  value of  $\sim 26\%$ , which is very close to the value obtained with the original method, as expected.

To assess how the methodology proposed here allows the analysis at atomic column resolution of regions with strong material segregation, where finding a reference area of known composition is challenging, another experimental sample that contains 30 ML of alternating layers of InSb/GaSb structures within a QD layer has been considered. The segregation tendency of In [45] tend to form  $\text{In}_x\text{Ga}_{1-x}\text{Sb}$  ternary alloy (ROI) and, hence, obtaining a reference area within the QD layer is rather challenging. On the other hand, due to a great distance of  $1.5 \mu\text{m}$  between the ROI and homogeneous GaSb buffer (reference), they cannot be imaged in the same micrograph. Therefore, it is impractical to quantify In using the original method. This limitation of the original qHAADF method is the principle encouraging factor to develop the modified method, enabling analyzing complex materials. HAADF-STEM images have been acquired from regions in the specimen along the curvature of the conventional technique generated hole, with the aim to find areas of similar thicknesses measured by zero-loss EELS. Figure 5a shows a HAADF-STEM image of the InSb/GaSb (ROI) region, and Fig. 5b depicts the corresponding absolute thickness profile calculated for electron MFP of  $\sim 61 \text{ nm}$  (calculated using the equations in [43]) at the spectrometer acceptance angle of  $90 \text{ mrad}$  (semi angle) using zero-loss EELS showing an average thickness of  $\sim 26 \text{ nm}$ . In order to calculate  $R$ , an area of similar thickness within the reference region (GaSb buffer) has been chosen. Figure 5c shows a HAADF-STEM image of the GaSb substrate, and Fig. 5d shows the absolute thickness profile within the white rectangle in Fig. 5c, generated similar way as in the ROI image. As observed in Fig. 5d, the average thickness at that white rectangle region in Fig. 5c is  $\sim 21 \text{ nm}$ . To ensure a slightly smaller thickness variation of the ROI area to the reference area, a smaller region ( $\sim 4 \text{ nm}$ ) in ROI image was chosen with an average thickness of  $\sim 25 \text{ nm}$ , as shown in the ROI thickness profile (Fig. 5b). Finally, the  $R$  map is generated on this new ROI using the modified method, illustrated in Fig. 5e. Here, the variable intensity in the group III atomic columns indicates heterogeneous In composition associated with In segregation within the image area. When the existing

ROI-reference average thickness variation of  $\sim 4 \text{ nm}$  is not considered, the maximum In composition in this region obtained using equation  $R = 1 + a \cdot x_i$  is  $\sim 18\%$ . In order to analyze how thickness contributes in the HAADF-STEM analyzed signal, simulated models of  $\text{GaSb}/\text{In}_x\text{Ga}_{1-x}\text{Sb}/\text{GaSb}$  have been generated. Figure 5f represents plots of  $R$  calculated for variable thicknesses of 21–27 nm on ROI in association with the average reference thickness of 21 nm in terms of 0–20% nominal In composition. Here, In associated increment factor has been found to be  $\sim 0.025 \pm 0.001$ . Now, with the help of the specimen thickness effect contributing equation mentioned above, the maximum In composition in Fig. 5e can be recalculated as  $\sim 3.27\%$ , as for each 1 nm specimen thickness variation, 3.75% false In composition is added in the HAADF-STEM signals. Local In composition values associated with each atomic column can be recalculated as well in order to obtain a precise information on the atomic column composition distribution in the material. Although it is out of the scope of this paper, this would allow a deep understanding of the growth process of the material, possible deviations from the original design due to segregation and the correlation to the functional properties of the material, which is often done using indirect techniques [13, 46].

## Conclusions

We have developed a modified qHAADF method for the quantitative analysis of the composition with atomic column resolution for cases where the ROI and the reference regions are imaged in separate HAADF-STEM micrographs. The compatibility of this method to the original method has been justified with the help of simulated HAADF-STEM images of  $\text{InAs}/\text{InSb}_x\text{As}_{1-x}/\text{InAs}$ , where  $0 \leq x \leq 0.5$ . The compatibility between the methods in terms of experimental InSb/InAs structures HAADF-STEM images has also been proved. Additionally, the significance of the modified method over the original method is justified in terms of HAADF-STEM compositional analysis of InSb/GaSb structure, situated far away from the homogeneous GaSb buffer layer.

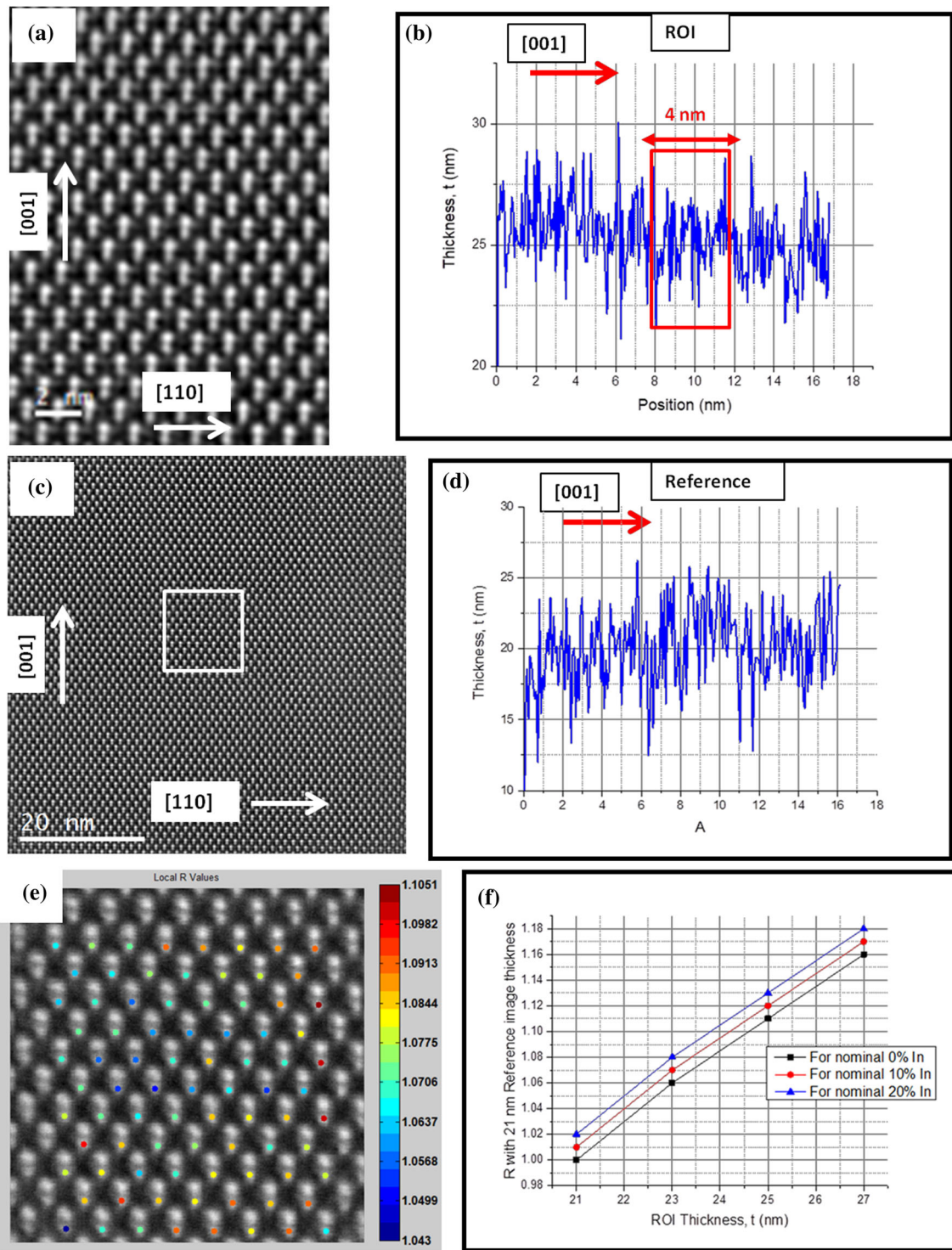


**Figure 5** **a** HAADF-STEM image of InSb/GaSb (ROI area) and **b** the corresponding absolute thickness profile; **c** HAADF-STEM image of the GaSb buffer layer (reference area) and **d** the corresponding thickness profile taken from the region on the white rectangle at **c**; **e** R map on the ~ 4 nm ROI area within the

selected thickness range in **b**, calculated with the modified method; **f** plots of In composition induced R versus specimen thickness effect as per simulated HAADF-STEM signals with ROI thicknesses of 21–27 nm in association with average reference thickness of 21 nm.

## Acknowledgements

This work was supported by European Union (UE) (postgraduate research on dilute metamorphic nanostructures and metamaterials in semiconductor photonics (PROMIS) Horizon 2020 initial training network (ITN) project), Spanish MINECO (Projects TEC2014-53727-C2-2-R and TEC2017-86102-C2-2-R) and the Junta de Andalucía (PAI research groups TEP-946 INNANOMAT and TIC-145). Cofinancing from UE-FEDER is also acknowledged.

## Compliance with ethical standards

**Conflict of interest** The authors declare that they do not have any conflict of interest.

## References

- [1] Pennycook SJ, Rafferty B, Nellist PD (2000) Z-contrast imaging in an aberration-corrected scanning transmission electron microscope. *Microsc Microanal* 6:343–352
- [2] Pennycook SJ, Boatner LA (1988) Chemically sensitive structure-imaging with a scanning electron microscope. *Nature* 336:565–567
- [3] Batson PE, Dellby N, Krivanek OL (2002) Sub-ångstrom resolution using aberration corrected electron optics. *Nature* 418:617–620
- [4] Muller DA, Nakagawa N, Ohtomo A, Grazul JA, Hwang HY (2004) Atomic-scale imaging of nanoengineered oxygen vacancy profiles in SrTiO<sub>3</sub>. *Nature* 430:657–661
- [5] Mitchson G, Ditto J, Woods KN, Westover R, Page CJ, Johnson DC (2016) Application of HAADF-STEM image analysis to structure determination in rotationally disordered and amorphous multilayered films. *Semicond Sci Technol* 31:084003
- [6] Kaiser U, Muller DA, Grazul JL, Chuvilin A, Kawasaki M (2002) Direct observation of defect-mediated cluster nucleation. *Nat Mater* 1:102–105
- [7] Yamazaki T, Nakanishi N, Recnik A, Kawasaki M, Watanabe K, Ceh M, Shiojiri M (2004) Quantitative high-resolution HAADF-STEM analysis of inversion boundaries in Sb<sub>2</sub>O<sub>3</sub>-doped zinc oxide. *Ultramicroscopy* 98:305–316
- [8] Anderson SC, Birkeland CR, Anstis GR, Cockayne DJH (1997) An approach to quantitative compositional profiling at near-atomic resolution using high-angle annular dark field imaging. *Ultramicroscopy* 69:83–103
- [9] Klie RF, Zhu Y (2005) Atomic resolution STEM analysis of defects and interfaces in ceramic materials. *Micron* 36:219–231
- [10] Klenov DO, Stemmer S (2006) Contributions to the contrast in experimental high-angle annular dark-field images. *Ultramicroscopy* 106:889–901
- [11] Wang P, Bleloch AL, Falke M, Goodhew PJ, Ng J, Missous M (2006) Direct measurement of composition of buried quantum dots using aberration-corrected scanning transmission electron microscopy. *Appl Phys Lett* 89:072111
- [12] Mokkaapati S, Jagadish C (2009) Review: III-V compound SC for optoelectronic devices. *Mater Today* 12:22–32
- [13] Semenov A, Lyublinskaya OG, Solov'ev VA, Meltser BY, Ivanov SV (2007) Surface segregation of Sb atoms during molecular-beam epitaxy of InSb quantum dots in an InAs(Sb) matrix. *J Cryst Growth* 301–302:58–61
- [14] Namazi L, Ghalamestani SG, Lehmann S, Zamani RR, Dick KA (2017) Direct nucleation, morphology and compositional tuning of InAs<sub>1-x</sub>Sb<sub>x</sub> nanowires on InAs (111) B substrates. *Nanotechnology* 28:165601
- [15] Zhang Y, Wu J, Aagesen M, Liu H (2015) Review: III-V nanowires and nanowire optoelectronic devices. *J Phys D Appl Phys* 48:463001
- [16] Bonef B, Gérard L, Rouvière JL, Grenier A, Jouneau PH, Bellet-Amalric E, Mariette H, André R, Bougerol C (2015) Atomic arrangement at ZnTe/CdSe interfaces determined by high resolution scanning transmission electron microscopy and atom probe tomography. *Appl Phys Lett* 106:051904
- [17] Tey CM, Liu HY, Cullis AG, Ross IM, Hopkinson M (2005) Structural studies of a combined InAlAs-InGaAs capping layer on 1.3- $\mu$ m InAs/GaAs quantum dots. *J Cryst Growth* 285:17–23
- [18] Chery N, Ngo TH, Chauvat MP, Damilano B, Courville A, Mierry PD, Grieb T, Mehrrens T, Krause FF, Caspary KM, Schowalters M, Gil B, Rosenauer A, Ruterana P (2017) The microstructure, local indium composition and photoluminescence in green-emitting InGaN/GaN quantum wells. *J Microsc* 00:1–8
- [19] Groiss H, Spindlberger L, Oberhumer P, Schäffler F, Fromherz T, Grydlik M, Brehm M (2017) Photoluminescence enhancement through vertical stacking of defect-engineered Ge on Si quantum dots. *Semicond Sci Technol* 32:02LT01
- [20] Nie JF (2017) IOP Conf Ser Mater Sci Eng 219:012005
- [21] Sales DL, Guerrero E, Rodrigo JF, Galindo PL, Yáñez A, Shafi M, Khatab A, Mari RH, Henini M, Novikov S, Chisholm MF, Molina SI (2011) Distribution of bismuth atoms in epitaxial GaAsBi. *Appl Phys Lett* 98:101902
- [22] Molina SI, Beltrán AM, Ben T, Galindo PL, Guerrero E, Taboada AG, Ripalda JM, Chisholm MF (2009) High resolution electron microscopy of GaAs capped GaSb nanostructures. *Appl Phys Lett* 94:043114
- [23] Broek WVD, Rosenauer A, Goris B, Martinez GT, Bals S, Aert SV, Dyck DV (2012) Correction of non-linear thickness

- in HAADF-STEM electron tomography. *Ultramicroscopy* 116:8–12
- [24] Rosenauer A, Gries K, Müller K, Pretorius A, Schowalter M, Avramescu A, Engl K, Lutgen S (2009) Measurement of specimen thickness and composition in Al<sub>x</sub>Ga<sub>1-x</sub>N/GaN using high-angle annular dark field images. *Ultramicroscopy* 109:1171–1182
- [25] Caspary KM, Oppermann O, Grieb T, Krause FF, Rosenauer A, Schowalter M, Mehrtens T, Beyer A, Volz K, Potapov P (2016) Material characterization by angle-resolved scanning transmission electron microscopy. *Sci Rep* 6:37146
- [26] LeBeau JM, Findlay SD, Allen LJ, Stemmer S (2008) Quantitative atomic resolution scanning transmission electron microscopy. *Phys Rev Lett* 100:206101
- [27] LeBeau JM, Findlay SD, Wang X, Jacobson AJ, Allen LJ, Stemmer S (2009) High-angle scattering of fast electrons from crystals containing heavy elements: simulation and experiment. *Phys Rev B* 79:214110
- [28] Martinez GT, Rosenauer A, Backer AD, Verbeeck J, Aert SV (2014) Quantitative composition determination at the atomic level using model-based high-angle annular dark field scanning transmission electron microscopy. *Ultramicroscopy* 137:12–19
- [29] Molina SI, Sales DL, Galindo PL, Fuster D, González Y, Alén B, González L, Varela M, Pennycook SJ (2009) Column-by-column compositional mapping by Z-contrast imaging. *Ultramicroscopy* 109:172–176
- [30] Molina SI, Galindo PL, Gonzalez L, Ripalda JM, Varela M, Pennycook SJ (2010) Exploring semiconductor quantum dots and wires by high resolution electron microscopy. *J Phys Conf Ser* 209:012004
- [31] Reyes DF, González D, Ulloa JM, Sales DL, Dominguez L, Mayoral A, Hierro A (2012) Impact of N on the atomic-scale Sb distribution in quaternary GaAsSbN-capped InAs quantum dots. *Nanoscale Res Lett* 7:653
- [32] Lu J, Luna E, Aoki T, Steenbergen EH, Zhang YH, Smith DJ (2016) Evaluation of Sb segregation in InAs/InAs<sub>1-x</sub>Sb<sub>x</sub> type-II superlattices grown by molecular beam epitaxy. *Appl Phys Lett* 119:095702
- [33] Pizarro J, Galindo PL, Guerrero E, Yáñez A, Guerrero MP, Rosenauer A, Sales DL, Molina SI (2008) Simulation of high angle annular dark field scanning transmission electron microscopy images of large nanostructures. *Appl Phys Lett* 93:153107
- [34] Molina SI, Guerrero MP, Galindo PL, Sales DL, Varela M, Pennycook SJ (2011) Calculation of integrated intensities in aberration-corrected Z-contrast images. *J Electron Microsc* 60:29–33
- [35] Galindo PL, Kret S, Sanchez AM, Laval JY, Yáñez A, Pizarro J, Guerrero E, Ben T, Molina SI (2007) The Peak Pairs algorithm for strain mapping from HRTEM images. *Ultramicroscopy* 107:1186–1193
- [36] Hernández-Maldonado D, Herrera M, Alonso-González P, González Y, González L, Gázquez J, Varlea M, Pennycook SJ, Guerrero-Lebrero MP, Pizarro J, Galindo PL, Molina SI (2011) Compositional analysis with atomic column spatial resolution by 5th-order aberration-corrected scanning transmission electron microscopy. *Microsc Microanal* 17:578–581
- [37] Jones L (2016) Quantitative ADF-STEM: acquisition, analysis and interpretation. *IOP Conf Ser Mater Sci Eng* 109:012008
- [38] MacArthur HE, MacArthur KE, Pennycook TJ, Okunishi E, D'Alfonso AJ, Lugg NR, Allen LJ, Nellist PD (2013) Probe integrated scattering cross sections in the analysis of atomic resolution HAADF STEM images. *Ultramicroscopy* 133:109–119
- [39] MacArthur KE, D'Alfonso AJ, Ozkaya D, Allen LJ, Nellist PD (2015) Optimal ADF STEM imaging parameters for tilt-robust image quantification. *Ultramicroscopy* 156:1–8
- [40] Martinez GT, Backer AD, Rosenauer A, Verbeeck J, Aert SV (2013) The effect of probe inaccuracies on the quantitative model-based analysis of high angle annular dark field scanning transmission electron microscopy images. *Micron* 63:57–63
- [41] Jones L, Nellist PD (2013) Identifying and correcting scan noise and drift in the scanning transmission electron microscope. *Microsc Microanal* 19:1050–1060
- [42] Aurenhammer F (1991) Voronoi diagrams—a survey of fundamental geometric data structure. *ACM Comput Surv* 23:345–405
- [43] Malis T, Cheng SC, Egerton RF (1988) EELS log-ratio technique for specimen-thickness measurement in the TEM. *J Electron Microsc* 8:193–200
- [44] Wiener N (1949) *Extrapolation, interpolation and smoothing of stationary time series*. Wiley, New York
- [45] Haxha V, Drouzas I, Ulloa JM, Bozkurt M, Koenraad PM, Mowbray DJ, Liu HY, Steer MJ, Hopkinson M, Migliorato MA (2009) Role of segregation in InAs/GaAs quantum dot structures capped with a GaAsSb strain-reduction layer. *Phys Rev B* 80:165334
- [46] Carrington PJ, Solov'ev VA, Zhuang Q, Krier A, Ivanov SV (2008) Room temperature midinfrared electroluminescence from InSb/InAs quantum dot light emitting diodes. *Appl Phys Lett* 93:091101